Appl Compos Mater (2018) 25:1369–1384
https://doi.org/10.1007/s10443-017-9671-z

# Insight into the Effects of Reinforcement Shape on Achieving Continuous Martensite Transformation in Phase Transforming Matrix Composites

**Xudong Zhang[1] · Junqiang Ren[2] · Xiaofei Wang[1] · Hongxiang Zong[1] · Lishan Cui[3] · Xiangdong Ding[1]**

Received: 8 December 2017 / Accepted: 11 December 2017 / Published online: 29 December 2017


**Abstract** A continuous martensite transformation is indispensable for achieving large linear superelasticity and low modulus in phase transforming metal-based composites. However, determining how to accurately condition the residual martensite in a shape memory alloy matrix though the reinforcement shape to achieve continuous martensite transformation has been a challenge. Here, we take the finite element method to perform a comparative study of the effects of nanoinclusion shape on the interaction and martensite phase transformation in this new composite. Two typical samples are compared: one reinforced by metallic nanowires and the other by nanoparticles. We find that the residual martensite within the shape memory alloy matrix after a pretreatment can be tailored by the reinforcement shape. In particular, our results show that the shape memory alloy matrix can retain enough residual martensite phases to achieve continuous martensite transformation in the subsequent loading when the aspect ratio of nanoreinforcement is larger than 20. In contrast, the composites reinforced with spherical or low aspect ratio reinforcement show a typical nonlinear superelasticity as a result of a low stress transfer-induced discontinuous martensite transformation within the shape memory alloy matrix.

✉ Xudong Zhang
xdzhangxjtu@163.com

✉ Hongxiang Zong
zonghust@mail.xjtu.edu.cn

✉ Xiangdong Ding
dingxd@mail.xjtu.edu.cn

[1] State Key Laboratory for Mechanical Behavior of Materials, Xi'an Jiaotong University, Xi'an 710049, China

[2] State Key Laboratory of Advanced Processing and Recycling of Non-ferrous Metals, Lanzhou University of Technology, Lanzhou 730050, China

[3] State Key Laboratory of Heavy Oil Processing, China University of Petroleum, Beijing 102249, China

**Keywords** Shape memory alloy · Composite · Stress transfer · Martensitic transformation

## 1 Introduction

Transforming metal nanocomposites, composed of a shape memory alloy (SMA) matrix with embedded nanoreinforcements, has been the subject of increasing attention because this unique design concept opens new frontiers in mechanical capabilities no conventional metallic matrix composites can achieve [1–3]. Different from conventional metallic matrix nanocomposites investigated before, in which the matrices deform plastically via dislocation slip [4–7], exploiting the intrinsic superior mechanical properties of nanoscale reinforcing materials in these matrices has proven to be challenging [8–10]; the SMA matrix deforms via a stress-induced martensitic transformation (SIMT) between austenite and martensite [11, 12], achieving the exceptional intrinsic properties of the nanoreinforcements [1, 13, 14]. Consequently, the transforming metal-based nanocomposite reinforced with large-aspect-ratio nanowires has achieved a combination of high strength, large quasi-linear superelasticity and low Young's modulus [1]. Given these superior properties, this composite has great potential for use in many applications such as dental braces, cardiac pacemakers, implantable devices, and flexible medical instruments [2].

The excellent mechanical properties of this composite are largely based on the continuous martensite transformation achieved in the SMA matrix [1], which can be ascribed to the contribution of the retained martensite phase generated by the interaction between the SMA matrix and reinforcements during pretreatment [1, 13, 15]. For such composites composed of a phase-transforming matrix, the interactions during the first loading process have been revealed in experimental works though stress transfer [14, 16–18]. In NiTi/CuZnAl-based composites, nanowires/fibers with large aspect ratios sustained an increasing stress fraction during SIMT [14, 17, 18]. The stress repartition caused by the plastic deformation of reinforcements has also been found in Mo fiber-reinforced CuZnAl composites [14]. Other experiments have shown that both R-phase reorientation and SIMT can cause stress repartition, with most of the stress being transferred from the SMA matrix to the elliptoid precipitates [16]. Upon unloading, the plastically deformed reinforcements hinder the recovery of the SMA matrix [1, 15], which results in an SMA with some retained martensite phase. However, the connect between the interaction created during unloading and the resulting residual martensite phase are currently unclear. Moreover, for a composite, the interaction between the components explicitly depends on the shape of the reinforcements [19, 20]. To provide effective stress transfer, the synthesis of such composites has always required intricate drawing technology to acquire an extremely large aspect ratio of the reinforcement [1, 13, 15]. If the shape of the reinforcements is more accessible, phase-transforming nanocomposites are expected to be more widely available. The aim of this paper is to explore the effect of reinforcement shape on achieving a continuous martensite phase transformation in a transforming metal-based composite.

In this work, we use the 3D finite element (FE) method to investigate the effects of reinforcement shape on the stress transfer within the composite during the mechanical pretreatment as well as the martensite phase transformation behavior in the subsequent loading process. Two kinds of reinforcements are studied, i.e., nanowires and spherical nanoparticles. The simulation indicates that the aspect ratio of the nanowires in phase-transforming matrix composites should not be less than 20 to provide sufficient stress transfer effects during pretreatment and preexisting martensite phases in the subsequent loading. In contrast, the reinforcing phase with this particle shape leads to a low effective stress transfer, deteriorating the mechanical performance of the composite.

## 2 Simulation Method

### 2.1 Representative Volume Element of SMA-Based Nanocomposites

According to the transmission electron microscopy images of the phase transforming matrix composites [1, 21], in which the SMA matrix can be regarded as a continuous medium without sharp grain boundaries at a scale of tens of nanometers. Thus, we utilized dimensionless continuum mechanics modeling to capture the microstructure and mechanical responses of the composites. The representative volume element (RVE) and random sequential adsorption algorithm approaches were used to capture the randomness of the reinforcements and generate the periodic geometries [22, 23]. Fig. 1a is an illustration of a longitudinal section of nanowires embedded in the SMA matrix. The nanowires are randomly dispersed in the SMA matrix and aligned along the axial direction of the composite wire. The end spacing between two nanowires is assumed to be twice the nanowire diameter. The nanowires are simplified into cylinders with a diameter $d = 60$ nm, and length of $L$. Several lengths ($L$) are selected to study the effect of aspect ratio ($L/d$) on the macroscopic mechanical response. The RVE model of the composite is defined as a cuboid with a length of $L + 2d$. The width and height of the cross-section is $h$ (Fig. 1c). For the nanoparticle-reinforced composite (Fig. 1b), the nanoparticles are simplified as spherical particles with diameter d = 60 nm and distributed randomly in the SMA matrix. The model is defined as a cube with a side length of $h$ (Fig. 1d). The volume fraction ($V_N$) of the nanoreinforcement is controlled by the number of inclusions.

The RVE method requires an appropriate definition of its domain, which should contain sufficient information of the microstructure up to a reasonable tolerance [24]. We examined the convergence of random RVEs at several scales (i.e., $h = 3d$, $6d$, $9d$, and $12d$). Given the trade-off relationship between efficiency and precision, the values of $h$ in all RVEs were selected to be $6d$. Although the aggregation of random nanoreinforcements has implications for the interfacial strength and mechanical properties of nanocomposites [25], there is no obvious debonding during the deformation according to the experiments of transforming metal-based nanocomposites [1, 15]. Therefore, a "perfect bonding" with coincident nodes at the inclusion–matrix interfaces was used to capture the properties of the interface.

### 2.2 Periodic Boundary Conditions

All the RVEs in our simulation were finely meshed into mixed C3D4 and C3D8 elements to ensure the accuracy of the simulated results (Fig. 1c, d). The mesh grids in the opposite boundary surfaces are the same so as to apply the periodic boundary conditions; this avoids unrealistic effects caused by the assumption of plane constraints as well as the size effect of the RVE [26, 27]. For the cuboid RVEs shown in Fig. 1c, d, the displacement field on a pair of opposite boundary surfaces is related to the strain field:

$$u_i^+ = \overline{\varepsilon}_{ik} l_k^+ + u_i^* \tag{1}$$

$$u_i^- = \overline{\varepsilon}_{ik} l_k^- + u_i^* \tag{2}$$

where $u_i^+$ and $u_i^-$ are the displacements for each pair of nodes located on opposite parallel boundary surfaces, $\overline{\varepsilon}_{ik}$ is the global strain tensor of the periodic structure, $l_k$ represents a linear

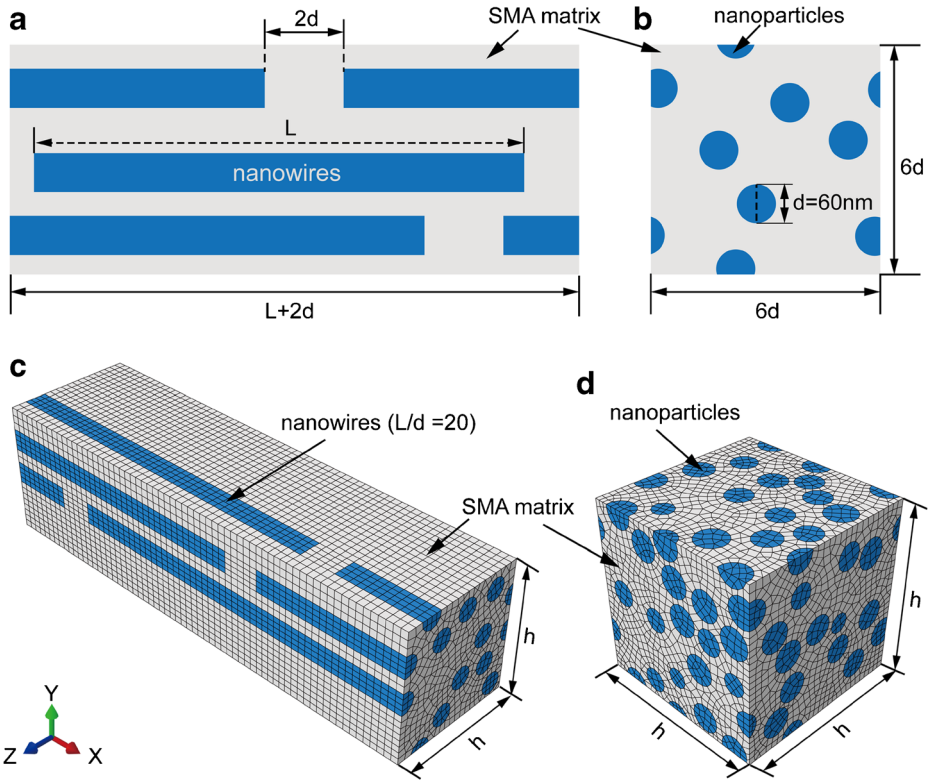


**Fig. 1** Schematic illustration of the periodic geometries of (**a**) nanowires and (**b**) nanoparticles embedded in the SMA matrix. **c** The RVE model of a nanowire-SMA composite with $L/d = 20$ and $V_N = 25\%$. **d** The RVE model of a nanoparticle-SMA composite with $V_N = 25\%$

distributed displacement field, and $u_i^*$ is the periodic part of the displacement components on the boundary surfaces. Then, the periodic boundary conditions can be defined by the difference between eqs. (1) and (2), as follows:

$$u_i^+ - u_i^- = \overline{\varepsilon}_{ik}\left(l_k^+ - l_k^-\right) = \overline{\varepsilon}_{ik}\Delta l_k \tag{3}$$

on the two parallel boundaries, $\Delta l_k$ is constant, with a specified $\overline{\varepsilon}_{ik}$, and the right side becomes constant. Therefore, a series of multi-point constraints can be performed by a Python code to constitute the periodic boundary conditions in the FE analysis. The application of eq. (3) guarantees the continuity conditions of displacement and stress field in the periodic structure [27].

### 2.3 Constitutive Model of the SMA Matrix

A phenomenological model based on Auricchio's work was used to simulate the superelastic-plastic behavior of the SMA matrix [28–30], which has been successful in capturing the mechanical behaviors of SMA composites [31, 32]. The constitutive model considers the superelastic behavior occurring during the reversible phase transformation between austenite

and detwinned martensite. The total strain is decomposed into three parts, including a purely linear elastic component ($\boldsymbol{\varepsilon}^e$), a transformation component ($\boldsymbol{\varepsilon}^t$), and a plastic strain ($\boldsymbol{\varepsilon}^p$),

$$\boldsymbol{\varepsilon} = \boldsymbol{\varepsilon}^e + \boldsymbol{\varepsilon}^t + \boldsymbol{\varepsilon}^p \tag{4}$$

The transformations strain ($\boldsymbol{\varepsilon}^t$) is induced by the martensitic transformation associated with an active reorientation process; thus, the transformation strain is constructed as the following equation:

$$\boldsymbol{\varepsilon}^t = \boldsymbol{\varepsilon}_L \xi_s \frac{\partial F(\boldsymbol{\sigma}, T)}{\partial \boldsymbol{\sigma}} \tag{5}$$

where $\boldsymbol{\varepsilon}_L$ is the maximum transformation strain, $\xi_s$ is the fraction of martensite, and $F(\boldsymbol{\sigma}, T)$ is the transformation potential that drives the martensitic transformation. This model introduces a Drucker-Prager type loading function for the reversible martensite transformation, as follows:

$$F(\boldsymbol{\sigma}, T) = \|\mathbf{t}\| + 3\alpha \mathrm{P\text{-}CT} \tag{6}$$

where $\mathbf{t}$ is the deviatoric part of the stress, which can be expressed as $\mathbf{t} = \boldsymbol{\sigma} - \mathrm{P}\mathbf{I}$. $\mathrm{P} = 1/3\boldsymbol{\sigma} : \mathbf{I}$ is the hydrostatic pressure, in which $\mathbf{I}$ is the second rank unit tensor. $\alpha$ and C are the material parameters, $\alpha$ describes the asymmetries of the transformation stress and strain between tension and compression, and C reflects the variation of stress levels with temperature. T is the temperature. So the temperature effect is included as well. The plastic strain ($\boldsymbol{\varepsilon}^p$) develops as soon as the material is loaded beyond the full austenite to martensite phase transformation. In this simulation, a linear strain-hardening plastic curve was used to define the yield behavior of the martensite phase:

$$\sigma = \sigma_s^y + E_p\left(\varepsilon - \sigma_s^y / E_M - \varepsilon_L\right) \quad \left(\sigma > \sigma_s^y\right) \tag{7}$$

where $\sigma_S^y$ is the yield stress of the SMA, $E_p$ represents the tangent modulus for plastic deformation, $\varepsilon$ is the macroscopic strain, $E_M$ is the elastic modulus of martensite, and $\varepsilon_L$ is the maximum superelastic strain. The superelastic-plastic behavior of the SMA matrix (Fig. 2) are defined by the parameters listed in Table 1.

## 3 Determining the Material Parameters and Validating the Simulation Method

Direct measurement of the constitutive material parameters of the reinforcement and the matrix at the nanoscale is impractical. However, some of their individual properties can be reasonably

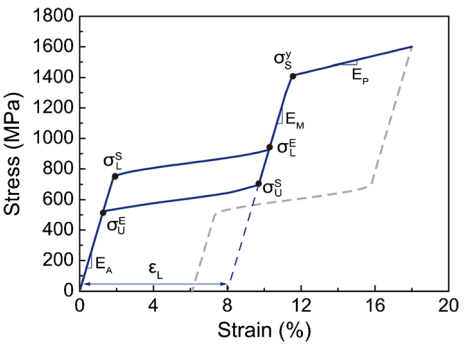


**Fig. 2** Stress-strain relationship for a NiTi material exhibiting a superelastic and plastic deformation

**Table 1** Summary of material coefficients for the SMA matrix

| Material parameter | Value |
|---|---|
| Austenite elastic modulus $E_A$ | 41 GPa |
| Martensite elastic modulus $E_M$ | 41 GPa |
| Tangent modulus for plastic deformation $E_p$ | 3 GPa |
| Starting stress for austenite to martensite transformation $\sigma_L^S$ | 738 MPa |
| Finishing stress for austenite to martensite transformation $\sigma_L^E$ | 940 MPa |
| Starting stress for martensite to austenite transformation $\sigma_U^S$ | 700 MPa |
| Finishing stress for martensite to austenite transformation $\sigma_U^E$ | 500 MPa |
| Yield stress of SMA $\sigma_S^y$ | 1400 MPa |
| Transformation strain $\varepsilon_L$ | 0.08 |

determined from the properties of the composite. From the stress-strain of the nanowire-SMA composite during the first loading [1], we determine that the Nb nanowires yielded after ~4.3% elastic lattice strain in the [110] direction. The elastic constant of bulk [110] Nb nanowires is 93 GPa [33]. Thus, the yield strength of a nanowire is estimated to be 93 GPa × 4.3% = 3.99 GPa. Our experimental results show that the particles precipitated by the aging method in the SMA matrix have a large elastic strain (~4.1%), which is close to the elastic limit of the nanowires (~4.3%) [1]. To facilitate a comparison, we assume that the spherical and wire-like inclusions possess the same elastic strain limits in the SMA matrix. Although anisotropic effects are to be expected at the nanometer scale, the mechanical responses obtained in our simulations are along the wire axial direction, which has the dominant effect, and it is almost impossible to estimate the anisotropic parameters of materials. Hence, the nanoinclusions are assumed to exhibit isotropic, perfect elastic-plastic behavior with an elasticity modulus ($E_R$) of 93 GPa, Poisson's ratio ($\nu_R$) of 0.33, and yield strength ($\sigma_{RS}$) of 3.99 GPa.

For the properties of the SMA matrix, the elastic modulus of the austenite can be determined by the rule of mixture. The elastic modulus of the composite during the first loading can be determined to be 54 GPa from the elastic region of the stress-stain curve for the composite [1]. Using the rule of mixture for parallel systems, $E_C = (1 - V_N)E_A + V_N E_R$, $E_C$, $E_A$ and $E_R$ are the elastic moduli of the composite, austenite and nanowires, respectively. $V_N$ is the volume fraction of nanowires and is 25% in this composite. Then, the elastic modulus of austenite in our system is estimated to be 41 GPa. It is also evident in Ref. 1 that a stress-induced martensitic transformation can occur in the SMA matrix at 1.8% lattice strain. Thus, the critical stress to induce the martensitic transformation in the SMA matrix $\left(\sigma_L^S\right)$ can be estimated to be 41 GPa × 1.8% = 0.738 GPa. The other material parameters were obtained by fitting the main features of the nanowire-SMA experiment [1]. All the values obtained through the above methods are consistent with the values reported in the literature [33–35]. The key parameters used to simulate the superelastic-plastic deformation of the SMA matrix are summarized in Table 1.

We then validate our simulation method with the experimental results [1], in which the nanowires have a mean aspect ratio exceeding 100. A volume fraction of $V_N$=25%, pretreatment strain of 9.5% (along the nanowire axial direction (x direction)), and aspect ratio of $L/d$ = 100 are selected to reproduce the experiment [1]. Figure 3a shows the evolution of strain for the nanowires and SMA matrix during the pretreatment. The strains of the nanowires and SMA matrix in our simulation were calculated according to the relationship between phase stress and lattice strain proposed by Refs. [14, 16–18, 36]. As shown in Fig. 3a, the varying trends of the simulation data (blue curve) are in good agreement with the actual measured data (red curve). We note that the curves show a tiny difference during unloading, which is caused

by the difference in the characterization approach. Upon unloading, the SMA matrix is mainly composed of martensite and gradually turns into a mixture of austenite and martensite phases. Our simulated curve of the SMA alloy describes the mixed state of the two-phase coexistence, while the experimental result estimated from the diffraction peaks of B2-NiTi (211) reflects the trend of the B2 austenite phase [1]. Figure 3b compares the tensile stress-strain curves of the nanowire-SMA composites at different temperatures during the second loading. After pre-treatment (Fig. 3b), the composites successfully achieve ultra-large elastic strains (>6%), low stiffness (~25.6 GPa) and high strengths (>1.65 GPa). Our simulation results (blue lines) approach the experimental ones (red lines) at 15 °C and 30 °C. At a higher temperature (50 °C), the elastic modulus of the experimental result is slightly higher than our simulated value. All these results indicate the current simulation method and constitutive law parameters are acceptable.

## 4 Results and Discussion

### 4.1 Effects of Reinforcement Shape on the Mechanical Behavior of the SMA-Based Composites

Figure 4a shows the stress-strain curves of the composites reinforced with various shapes of reinforcements during pretreatment (9.5% pre-strain). The volume fraction of the reinforcements is 25%. We find that the composites display a two-yield phenomenon (points A and B) during the loading process when the aspect ratio of the nanowires exceeds 10. The onset of SIMT in the SMA matrix and plastic deformation within the nanowires lead to the first yield point (point A) and the second yield point (point B), respectively. With further increases of the nanowire aspect ratio ($L/d \geq 20$), the composites exhibit almost the same deformation behavior during pretreatment, including the macro-stress of phase transformation (~900 MPa, point A), the second yield stress (~1550 MPa, point B), maximum stress at pre-strain of 9.5% (~1650 MPa, point C), and the value of the residual strain (~3%, point F).

In the subsequent loading process (Fig. 4b), the composites reinforced by nanowires with large aspect ratios (≥20) exhibit large quasi-linear superelasticity. However, the composites reinforced by

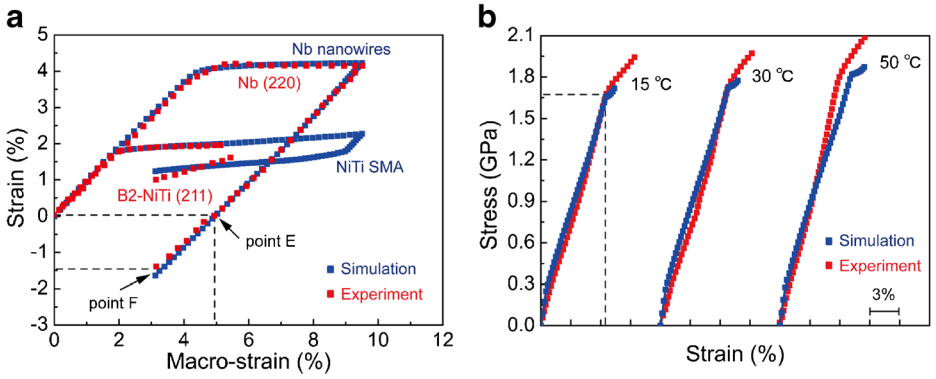


**Fig. 3** Comparisons between experimental [1] and simulated results, showing the validity of the implemented simulation method. **a** Evolutions of strain for nanowires and the SMA matrix during the pretreatment. **b** Tensile stress-strain curves of the composites during the subsequent tensile cycle at different temperatures

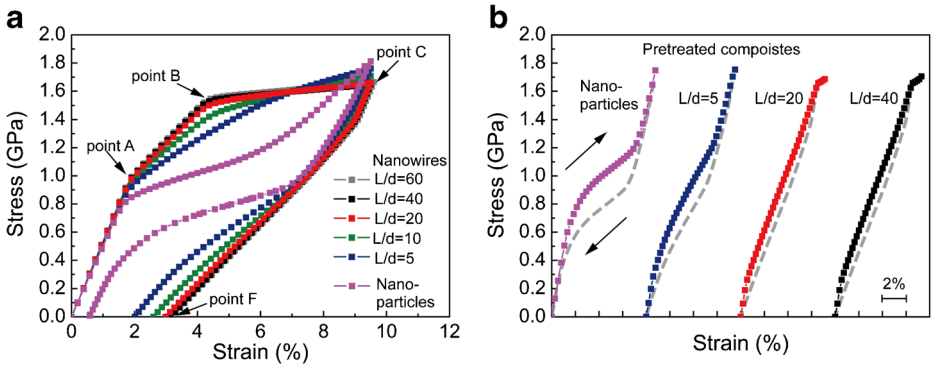


**Fig. 4** **a** Cyclic stress-strain curves of the composites during the pretreatment cycle. **b** Tensile stress-strain curves of the composites during the subsequent loading

nanowires with low aspect ratios (e.g., $L/d = 5$) or nanoparticles show a typical nonlinear behavior, indicating that the aspect ratio of the nanowires could be appropriately reduced to 20 without losing the strengthening effect of the nanoreinforcements. It should be noted that the strengthening mechanisms in a nanocomposite are complex. However, the interaction between the forward/reverse phase transformation of the SMA matrix and the elastic-plastic deformation of the reinforcement play a dominant role in enhancing the properties of phase transforming-based composite materials [1, 13]. In the following sections, we explore the relationship among reinforcement shape, stress transfer effect, martensite transformation behavior, and the mechanical properties of the phase transforming-based composites.

## 4.2 Stress Transfer Characteristics During the Loading Process

The interaction between reinforcements and a matrix enables each component to share the external load, which can be characterized by stress transfer [37, 38]. The stress transfer in our simulation is calculated by $V_{phase}\sigma_{phase}/\sigma_c$ according to the definition proposed by Refs. [14, 16–18, 36], which is defined as the stress fraction carried by each phase. $\sigma_{phase}$, $\sigma_c$, and $V_{phase}$ are the average von Mises stress of each phase, macro-stress of the composite, and volume fraction of each phase, respectively. The stress fractions carried by the nanoreinforcements and the corresponding SMA matrix as a function of macroscopic strain during first loading are shown in Fig. 5.

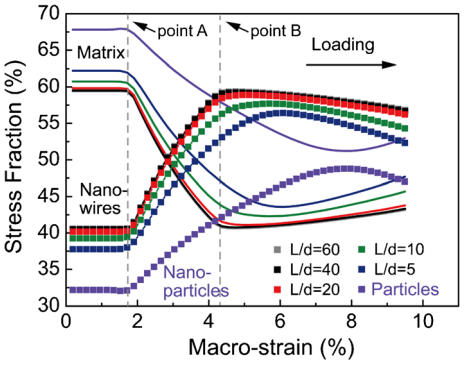


**Fig. 5** The stress fractions carried by nanowires with different aspect ratios and nanoparticles as a function of macroscopic strain upon tensile loading

As shown in Fig. 5, the stress carried by the nanoreinforcements and SMA matrix remains constant in the initial elastic stage (before point A), which reveals that the stress transfer effect remains unchanged when the components undergo elastic deformation. When the SMA matrix undergoes SIMT, the stress fraction carried by the reinforcements increases rapidly with the macro-strain, indicating that SIMT causes the stress to transfer from the matrix to the reinforcements. When the aspect ratio is over 20, the efficiency is nearly saturated, which is similar to that presented in Fig. 4a. When the macroscopic strain approaches ~4.3% (the elastic strain limit of the reinforcements, point B), even though the nanowires ($L/d \geq 20$) only have a low volume fraction (25%), they bear more than half of the stress (~60%). With further loading, the stress fraction of the nanowires decreases gently (after point B), which indicates that the plastic deformation in reinforcements can give rise to stress repartition. The stress fraction carried by the SMA matrix shows an opposite trend. The stress transfer characteristics in transforming metal-based nanocomposites during the first loading process have been confirmed in previous experimental works [14, 16–18]. R-phase reorientation, SIMT and the plastic deformation of reinforcements can all cause stress repartition. The calculated stress transfer characteristics are consistent with those observed experimentally.

We note that the stress repartition caused by the plasticity of reinforcements is postponed with the decreasing nanowire aspect ratio, indicating that nanowires with small aspect ratios or nanoparticles do not undergo evident plastic deformation during the loading process. Here, we compared the equivalent plastic strain of each component in two typical models ($V_N$=25%) at a macro-strain of 9.5%. Figure 6(a1) shows that almost all the nanowires ($L/d=20$) exhibit plastic deformation, while because of the inefficient stress transfer, only a small part of the nanoparticles (Fig. 6(b1)) are in the plastic region. This insufficient plastic deformation within the nanoparticles cannot cause a strong interaction with the reverse transformation of the SMA matrix during unloading (Fig. 7, purple curves), resulting in a few martensite regions remaining in the matrix (Fig. 8). Figure 6 also reveals that the plasticity occurs only between the ends of two nanowires in the SMA matrix (Fig. 6(a2), black arrows). However, severe plastic deformation occurs within many regions of the SMA matrix reinforced by nanoparticles (Fig. 6(b2)). This indicates that a serious stress concentration exists in the nanoparticle-reinforced SMA composites.

### 4.3 Stress Transfer during Unloading and its Effect on the Residual Martensite within the SMA Matrix

The stress transfer during unloading is caused by the interaction between the plastically deformed reinforcements and the reverse transformation of the SMA matrix. Upon unloading (Fig. 7), the

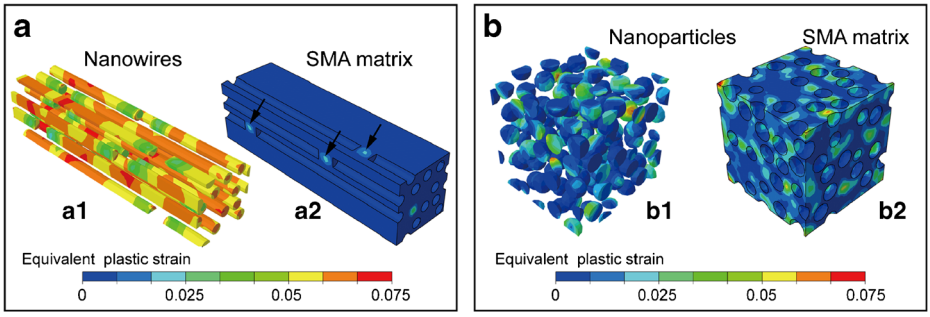


**Fig. 6** Equivalent plastic strain within the reinforcements and corresponding SMA matrix at a macro-strain of 9.5%. **a** Nanowires and corresponding SMA matrix. **b** Nanoparticles and corresponding SMA matrix

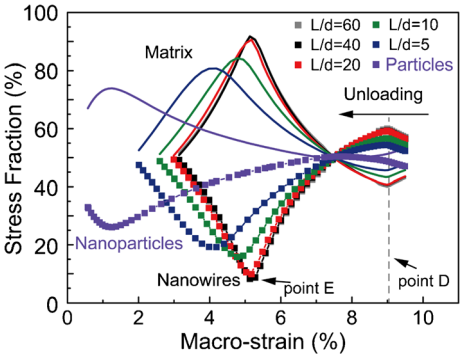


**Fig. 7** The stress fractions carried by nanowires with different aspect ratios and nanoparticles as a function of macroscopic strain upon unloading

tensile elastic strains and the corresponding stress within the components relax. The saturated stress transfer effect also exists in the unloading process when the aspect ratio of the nanowires exceeds 20, which indicates that the interaction caused by plastically deformed nanowires and the reverse phase transformation of the SMA matrix is almost the same when the aspect ratio is larger than 20. The stress fraction carried by the nanowires increases at first and then decreases rapidly. This stress repartition (point D) is due to the initiation of a reverse transformation from martensite to the parent phase. During the reverse transformation, the SMA matrices reinforced by large-aspect-ratio nanowires carry an increasing fraction of stress up to ~90% (drops to ~10% for nanowires) when the macro-strain reaches ~5% (point E). Due to the mismatch in the recoverable strains of the SMA matrix and reinforcements [15], a reversal of the strain state within the nanowires from tension to compression (Fig. 3a, points E to F) occurs. At the same time, the stress is reallocated to the nanowires. This sharp stress repartition reveals the strong interaction between the plastically deformed nanowires and the phase-transforming SMA matrix. However, the stress repartition gradually slows down with decreasing aspect ratio, which means that the interaction between the components becomes weaker, and the nanoparticle-reinforced composite generates the weakest interaction between the components.

The residual martensite is created due to the interaction during the unloading process. As shown in Fig. 8, we calculated the average volume fraction of the martensite phase within the SMA matrices reinforced with nanoparticles and nanowires (aspect ratios ranging from 1 to 40) after pretreatment. As we expected, there is almost no residual martensite in the SMA matrix reinforced by nanoparticles or nanowires with $L/d = 1$ due to the weak interaction. The mean residual martensite fraction first increases with the aspect ratio and then remains at a constant value

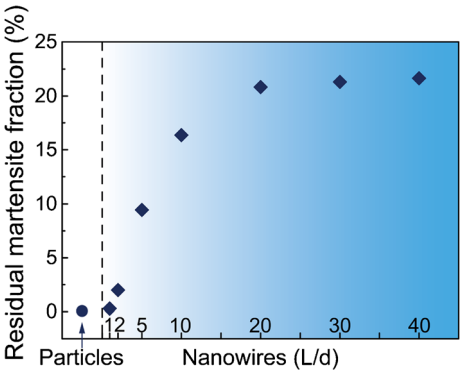


**Fig. 8** Effect of the shape of reinforcements on the average residual martensite phase volume fraction within the SMA matrix after pretreatment

(~21%) when the aspect ratio is greater than 20, which is consistent to the stress transfer effect during pretreatment. This also reveals the underlying cause of the same quasi-linear superelastic behavior of the composites when the nanowire aspect ratio exceeds 20 (Fig. 4b).

### 4.4 Stress Transfer Characteristics and Martensitic Transformation during Subsequent Loading

For the stress transfer characteristics that occur during the subsequent loading process, we present a comparison of the nanowire-reinforced composite ($L/d$=20) with the nanoparticle-reinforced one. For the nanoparticle-reinforced composite (Fig. 9a), clearly, the slight strain relaxation cannot cause stress repartition (blue region). After the initiation of local SIMT (point G), the stress fraction of the nanoparticles (red line) increases continuously, which means that the stress transfers from the SMA matrix to the nanoparticles heavily during SIMT. This is similar to that of the first loading process in SMA-based composites (Fig. 5). For the composite reinforced with nanowires (Fig. 9b), at the beginning, the stress fraction carried by the nanowires decreases rapidly (red line), while the stress fraction of the SMA matrix (blue line) increases continuously until the macro-strain is ~2.1%. Then, the nanowires start to bear a tensile load, and the stress is reassigned to the nanowires. This stress repartition is due to the relaxation of elastic compressive strain in the nanowires. The stress repartition occurring at the macro-strain of ~6.5% (point H) is caused by plastic deformation within the nanowires. We note that the initiation of SIMT does not significantly redistribute the stress fraction (point G), which is different from that of the first loading process in bulk nanowire-SMA composites [14, 16–18] and the subsequent loading in nanoparticle-SMA composites (Fig. 9a).

The difference in the stress transfer way can be attributed to the difference in martensite phase transformation. As shown in Fig. 10a, for the SMA matrix reinforced with nanoparticles, because of the very weak interaction during unloading (as shown in Fig. 7, purple curves), only a few residual martensite nuclei (Fig. 10(a1), yellow arrows) are generated in the SMA matrix by stress concentration during the recovery of the SMA matrix rather than its interaction with the plasticity of the nanoparticles. With further loading, as shown in Fig. 10(a2-a4), the martensitic transformation is not initiated from the growth of the preexisting residual martensite nuclei (red circles). This indicates that the martensitic transformation within the SMA

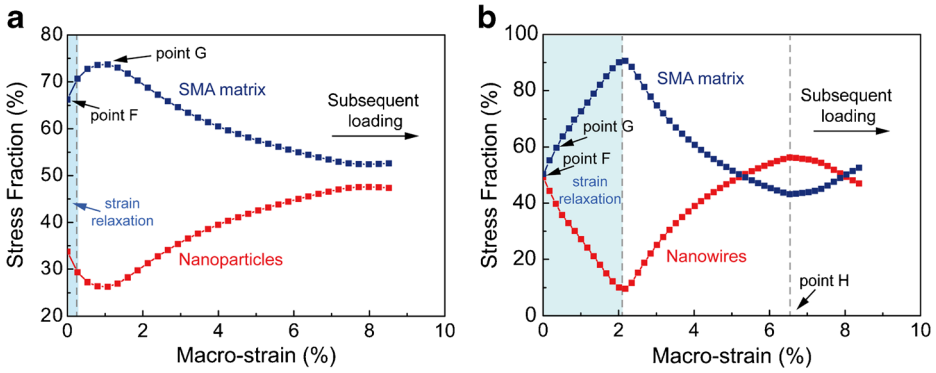


**Fig. 9** The stress fractions carried by (**a**) nanoparticles and the corresponding SMA matrix and (**b**) nanowires ($L/d$=*20*) and the corresponding SMA matrix as a function of macroscopic strain during the subsequent loading. Points F and G in Fig. 9 point to the initial state of the SMA matrix and the emergence of martensite in the second loading, respectively

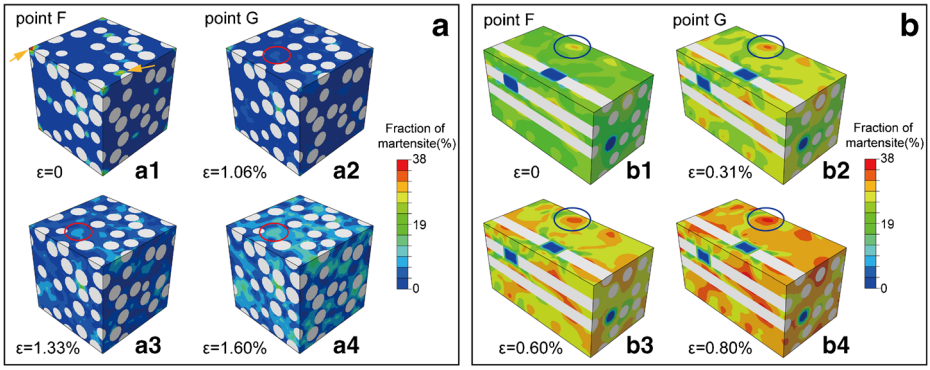


**Fig. 10** Evolution of the martensite phase transformation in the subsequent loading process. **a** The SMA matrix reinforced by nanoparticles; the red circles point to the nucleation and increase of the martensite phase. **b** The SMA matrix reinforced by nanowires ($L/d$=20); the blue circles point to the increase and expansion of the martensite phase (shows only 1/2 of the model along the axial direction). Points F-G and strains in Fig. 10a, b correspond to the locations in Fig. 9a, b, respectively

matrix reinforced by nanoparticles occurs discontinuously. However, for nanowire-reinforced composites (Fig. 10b), nearly all the SMA matrix is in austenite-martensite coexistence because of the strong interaction during pretreatment (Fig. 10(b1)). In the subsequent loading, as indicated by the blue circles in Fig. 10(b2-b4), the volume fraction of martensite first increases and expands from the area that contains more retained martensite regions, which indicates that the martensite grows directly from the preexisting martensite, leading to a more continuous martensite phase transformation behavior. It is further revealed that the stress transfer effect caused by a continuous SIMT is significantly weaker than a discontinuous phase transformation.

### 4.5 Effects of Martensite Phase Transformation on the Superelastic Properties

The continuous martensite transformation, on the one hand, provides an extremely low modulus for the composite. The stress repartition during SIMT is actually caused by the change of modulus from elastic deformation to the SIMT transition [14]. Therefore, the stress repartition disappearing during continuous SIMT (Fig. 9b) implies that the tangential modulus

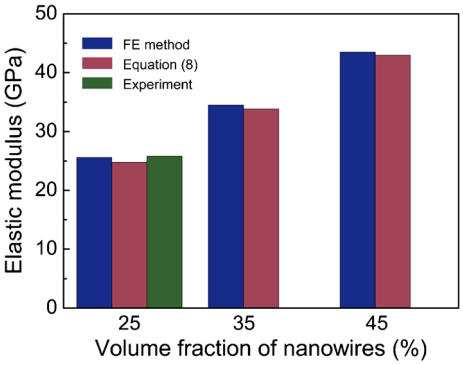


**Fig. 11** Comparison of the elastic moduli of the continuous phase transforming-based nanocomposites predicted by the FE method and modified rule of mixture as well as that measured experimentally from the pretreated composites [1]

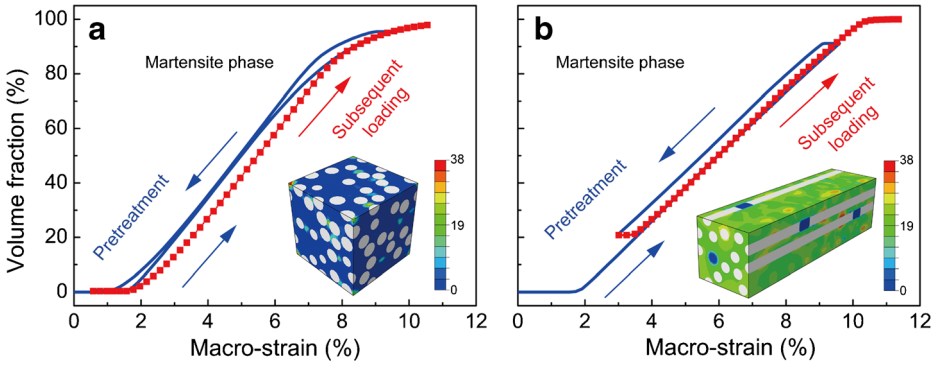


**Fig. 12** Evolution of average volume fraction of the martensite phase during the pretreatment and the subsequent loading process. **a** The SMA matrix reinforced by nanoparticles. **b** The SMA matrix reinforced by nanowires ($L/d = 20$). (Inset) Distributions of martensite volume fractions after pretreatment

of the SMA matrix remains relatively unaltered. The elastic modulus of the continuous phase transforming-based nanocomposite can be estimated by a modified rule of mixture:

$$E_C = V_N E_R + (1 - V_N) E_M^t \tag{8}$$

where $V_N$ and $E_R$ are the volume fraction and elastic modulus of the reinforcement, respectively, and $E_M^t$ is the tangential modulus of the SMA matrix during continuous SIMT. We already know $V_N = 25\%$ and $E_R = 93$ GPa. The tangential modulus $E_M^t = 2$ GPa is estimated from the slope of the upper stress plateau during the martensite transformation (Fig. 2). The calculated elastic modulus of the composite is 24.75 GPa. This value agrees very well with the previous experimental result [1]. In addition, according to eq. (8), enhancing the interaction by increasing the volume fraction of nanowires will cause an increase in the composite elastic modulus, as shown in Fig. 11.

On the other hand, the continuous SIMT provides the quasi-linear elastic behavior of the composite. For the SMA matrix containing a few retained martensite phases (Fig. 12a), for example, the composites reinforced with nanoparticles, most constituents of the SMA undergo a lengthy initial elastic deformation followed by an abrupt discontinuous SIMT transition during the subsequent loading (red line), leading to the typical nonlinear superelasticity of the composite (Fig. 4b). The phase transformation within the matrix occurs more continuously with increasing retained martensite. When the SMA matrix retains a certain number of martensite regions (i.e., austenite-martensite coexistence) after pretreatment (Fig. 12b, inset), the martensitic phase grows from the preexisting martensite cores, so the average volume fraction of the martensite phase increases almost continuously in the subsequent loading (Fig. 12b, red line). The SMA matrix undergoes continuous SIMT [1], and then quasi-linear superelasticity of the composite is achieved.

## 5 Conclusions

In summary, our results showed that the shape of reinforcement played an important role in determining the mechanical behaviors of phase-transforming composites. When the aspect ratio of the nanowires exceeded 20, the composites exhibited similar efficient

stress transfers and the SMA matrix retained adequate residual martensite after pretreatment, which gave rise to continuous SIMT and large quasi-linear superelasticity during the subsequent loading process. In contrast, the composites reinforced by nanowires with a low aspect ratio or nanoparticles generated an insufficient stress transfer effect during pretreatment and, thus, a discontinuous martensite transformation in the subsequent loading process, which cannot help the SMA to achieve a linear superelasticity. We revealed the stress transfer characteristics of the entire cycle loading process, providing a more comprehensive understanding of the role of the interaction between the components within phase transforming material-based composites.

**Acknowledgements** The authors wish to appreciate the support of the National Natural Science Foundation of China (51231008, 51320105014, 51501141) and 111 project (B06025). X. Z acknowledges the computational resources provided by the HPC platform of Xi'an Jiaotong University.

## References

1. Hao, S., Cui, L., Jiang, D., Han, X., Ren, Y., Jiang, J., Liu, Y., Liu, Z., Mao, S., Wang, Y., Li, Y., Ren, X., Ding, X., Wang, S., Yu, C., Shi, X., Du, M., Yang, F., Zheng, Y., Zhang, Z., Li, X., Brown, D.E., Li, J.: A transforming metal nanocomposite with large elastic strain, low modulus, and high strength. Science. **339**(6124), 1191–1194 (2013). https://doi.org/10.1126/science.1228602
2. Zhou, M.: Exceptional properties by design. Science. **339**(6124), 1161–1162 (2013). https://doi.org/10.1126/science.1236378
3. Li, J., Shan, Z., Ma, E.: Elastic strain engineering for unprecedented materials properties. MRS Bull. **39**(02), 108–117 (2014). https://doi.org/10.1557/mrs.2014.3
4. Chen, Y., Liu, Y., Sun, C., Yu, K.Y., Song, M., Wang, H., Zhang, X.: Microstructure and strengthening mechanisms in Cu/Fe multilayers. Acta Mater. **60**(18), 6312–6321 (2012). https://doi.org/10.1016/j.actamat.2012.08.005
5. Thilly, L., Petegem, S.V., Renault, P.O., Lecouturier, F., Vidal, V., Schmitt, B., Swygenhoven, H.V.: A new criterion for elasto-plastic transition in nanomaterials: application to size and composite effects on Cu–Nb nanocomposite wires. Acta Mater. **57**(11), 3157–3169 (2009). https://doi.org/10.1016/j.actamat.2009.03.021
6. Sun, Y., Sun, J., Liu, M., Chen, Q.: Mechanical strength of carbon nanotube–nickel nanocomposites. Nanotechnology. **18**(50), 505704 (2007). https://doi.org/10.1088/0957-4484/18/50/505704
7. Thilly, L., Renault, P.O., Vidal, V., Lecouturier, F., Van Petegem, S., Stuhr, U., van Swygenhoven, H.: Plasticity of multiscale nanofilamentary Cu/Nb composite wires during in situ neutron diffraction: Codeformation and size effect. Appl. Phys. Lett. **88**(19), 191906 (2006). https://doi.org/10.1063/1.2202720
8. Dzenis, Y.: Structural nanocomposites. Science. **319**(5862), 419–420 (2008). https://doi.org/10.1126/science.1151434
9. Podsiadlo, P., Kaushik, A.K., Arruda, E.M., Waas, A.M., Shim, B.S., Xu, J., Nandivada, H., Pumplin, B.G., Lahann, J., Ramamoorthy, A., Kotov, N.A.: Ultrastrong and stiff layered polymer nanocomposites. Science. **318**(5847), 80–83 (2007). https://doi.org/10.1126/science.1143176
10. Coleman, J.N., Khan, U., Gun'ko, Y.K.: Mechanical reinforcement of polymers using carbon nanotubes. Adv. Mater. **18**(6), 689–706 (2006). https://doi.org/10.1002/adma.200501851
11. Otsuka, K., Ren, X.: Physical metallurgy of Ti–Ni-based shape memory alloys. Prog. Mater. Sci. **50**(5), 511–678 (2005). https://doi.org/10.1016/j.pmatsci.2004.10.001
12. Otsuka, K., Wayman, C.M.: Shape Memory Materials. Cambridge University Press, Cambridge (1998)
13. Hao, S., Cui, L., Guo, F., Liu, Y., Shi, X., Jiang, D., Brown, D.E., Ren, Y.: Achieving large linear elasticity and high strength in bulk nanocompsite via synergistic effect. Sci. Rep. **5**(1), 8892 (2015). https://doi.org/10.1038/srep08892
14. Yang, F., Ni, D., Hao, S., Li, S., Ma, Z., Liu, Y., Feng, C., Cui, L.: Microstructure and phase stress partition of Mo fiber reinforced CuZnAl composite. Mater. Sci. Eng. A. **628**, 419–422 (2015). https://doi.org/10.1016/j.msea.2015.01.068

15. Liu, Z., Cui, L., Liu, Y., Jiang, D., Jiang, J., Shi, X., Shao, Y., Zheng, Y.: Influence of internal stress coupling on the deformation behavior of NiTi-Nb nanowire composites. Scripta Mater. **77**, 75–78 (2014). https://doi.org/10.1016/j.scriptamat.2014.01.027
16. Dong, Y., Cong, D., Nie, Z., He, Z., Li, L., Wang, Z., et al.: Stress transfer during different deformation stages in a nano-precipitate-strengthened Ni-Ti shape memory alloy. Appl. Phys. Lett. **107**(20), 201901 (2015). https://doi.org/10.1063/1.4935691
17. Hao, S.J., Jiang, D.Q., Cui, L.S., Wang, Y.D., Shi, X.B., Nie, Z.H., Brown, D.E., Ren, Y.: Phase-stress partition and stress-induced martensitic transformation in NbTi/NiTi nanocomposite. Appl. Phys. Lett. **99**(8), 084103 (2011). https://doi.org/10.1063/1.3629768
18. Yu, C., Liu, Z., Liu, Y., Shao, Y., Ren, Y., Cui, L.: Load transfer in phase transforming matrix–nanowire composite revealing the significant load carrying capacity of the nanowires. Mater. Des. **89**, 721–726 (2016). https://doi.org/10.1016/j.matdes.2015.10.029
19. Li, Y., RAMESH, K.T.: Influence of particle volume fraction, shape, and aspect ratio on the behavior of particle-reinforced metal–matrix composites at high rates of strain. Acta Mater. **46,** 5633-5646 (1998). https://doi.org/10.1016/S1359-6454(98)00250-X
20. Xin, L., Yang, W., Zhao, Q., Dong, R., Liang, X., Xiu, Z., Hussain, M., Wu, G.: Effect of extrusion treatment on the microstructure and mechanical behavior of SiC nanowires reinforced al matrix composites. Mater. Sci. Eng. A. **682**, 38–44 (2017). https://doi.org/10.1016/j.msea.2016.11.042
21. Hao, S., Cui, L., Wang, H., Jiang, D., Liu, Y., Yan, J., Ren, Y., Han, X., Brown, D.E., Li, J.: Retaining large and adjustable elastic strains of kilogram-scale Nb nanowires. ACS Appl. Mater. Interfaces. **8**(5), 2917–2922 (2016). https://doi.org/10.1021/acsami.5b10840
22. Segurado, J., Llorca, J.: A numerical approximation to the elastic properties of sphere-reinforced composites. J. Mech. Phys. Solids. **50**(10), 2107–2121 (2002). https://doi.org/10.1016/S0022-5096(02)00021-2
23. Tian, W., Qi, L., Zhou, J., Guan, J.: Effects of the fiber orientation and fiber aspect ratio on the tensile strength of $C_{sf}$ /Mg composites. Comput. Mater. Sci. **89**, 6–11 (2014). https://doi.org/10.1016/j.commatsci.2014.03.004
24. Mirkhalaf, S.M., Andrade Pires, F.M., Simoes, R.: Determination of the size of the representative volume element (RVE) for the simulation of heterogeneous polymers at finite strains. Finite Elem. Anal. Des. **119**, 30–44 (2016). https://doi.org/10.1016/j.finel.2016.05.004
25. Zare, Y., YopRhee, K., Hui, D.: Influences of nanoparticles aggregation/agglomeration on the interfacial/interphase and tensile properties of nanocomposites. Compos. Pt. B-Eng. **122**, 41–46 (2017). https://doi.org/10.1016/j.compositesb.2017.04.008
26. Xia, Z., Zhang, Y., Ellyin, F.: A unified periodical boundary conditions for representative volume elements of composites and applications. Int. J. Solids Struct. **40**(8), 1907–1921 (2003). https://doi.org/10.1016/S0020-7683(03)00024-6
27. Xia, Z., Zhou, C., Yong, Q., Wang, X.: On selection of repeated unit cell model and application of unified periodic boundary conditions in micro-mechanical analysis of composites. Int. J. Solids Struct. **43**(2), 266–278 (2006). https://doi.org/10.1016/j.ijsolstr.2005.03.055
28. Auricchio, F., Taylor, R.L.: Shape-memory alloys: modelling and numerical simulations of the finite-strain superelastic behavior. Comput. Methods Appl. Mech. Eng. **143**(1-2), 175–194 (1997). https://doi.org/10.1016/S0045-7825(96)01147-4
29. Auricchio, F., Taylor, R.L., Lubliner, J.: Shape-memory alloys: macromodelling and numerical simulations of the superelastic behavior. Comput. Methods Appl. Mech. Eng. **146**(3-4), 281–312 (1997). https://doi.org/10.1016/S0045-7825(96)01232-7
30. Gong, X., Pelton, A.: ABAQUS Analysis on Nitinol Medical Applications. SMST Society, California (2002)
31. Lei, H., Wang, Z., Zhou, B., Tong, L., Wang, X.: Simulation and analysis of shape memory alloy fiber reinforced composite based on cohesive zone model. Mater. Des. **40**, 138–147 (2012). https://doi.org/10.1016/j.matdes.2012.03.037
32. Lei, H., Wang, Z., Tong, L., Zhou, B., Fu, J.: Experimental and numerical investigation on the macroscopic mechanical behavior of shape memory alloy hybrid composite with weak interface. Compos. Struct. **101**, 301–312 (2013). https://doi.org/10.1016/j.compstruct.2013.02.006
33. Cohen, D.E., Bevk, J.: Enhancement of the Young's modulus in the ultrafine Cu-Nb filamentary composites. Appl. Phys. Lett. **39**(8), 595–597 (1981). https://doi.org/10.1063/1.92842
34. Nemat-Nasser, S., Guo, W.: Superelastic and cyclic response of NiTi SMA at various strain rates and temperatures. Mech. Mater. **38**(5-6), 463–474 (2006). https://doi.org/10.1016/j.mechmat.2005.07.004
35. Machado, G., Louche, H., Alonso, T., Favier, D.: Superelastic cellular NiTi tube-based materials: fabrication, experiments and modeling. Mater. Des. **65**, 212–220 (2015). https://doi.org/10.1016/j.matdes.2014.09.007

36. Jiang, J., Jiang, D., Hao, S., Yu, C., Zhang, J., Ren, Y., Lu, D., Xie, S., Cui, L.: A nano lamella NbTi–NiTi composite with high strength. Mater. Sci. Eng. A. **633,** 121–124 (2015). https://doi.org/10.1016/j.msea.2015.03.010
37. Jia, Z., Ma, H., Cheng, L., Lau, K., Hui, D., Yuan, G.: Stress transfer properties of carbon nanotube reinforced polymer composites at low temperature environment. Compos. Pt. B-Eng. **106**, 356–365 (2016). https://doi.org/10.1016/j.compositesb.2016.09.006
38. Mohonee, V.K., Goh, K.L.: Effects of fibre-fibre interaction on stress uptake in discontinuous fibre reinforced composites. Compos. Pt. B-Eng. **86**, 221–228 (2016). https://doi.org/10.1016/j.compositesb.2015.10.015